Construction and Building Materials 335 (2022) 127528

Contents lists available at ScienceDirect

Construction and Building Materials

journal homepage: www.elsevier.com/locate/conbuildmat

Hydration mechanisms and mechanical properties of pumice substituted cementitious binder

İbrahim Pınarcı [a], Yilmaz Kocak [b,*]

[a] Bilecik Seyh Edebali University, Pazaryeri Vocational School, Department of Design, Turkey
[b] Duzce University, Faculty of Engineering, Department of Civil Engineering, Turkey

ARTICLE INFO

Keywords:
Portland cement
Pumice
Compressive strength
Hydration
Microstructure

ABSTRACT

This paper reports the hydration production, micro structuring, and compressive strength results of Portland cement–pumice systems. The compressive strengths of cement mortars examined on the 2nd, 7th, 28th, and 90th days in the first stage. In the second step, hydration mechanisms of cement paste samples containing 0%, 10%, and 20% pumice at the 2nd, 7th, 28th, and 90th ages were determined by SEM, FT–IR, XRD, and DTA/TGA. In addition, the chemical, physical, molecular, mineralogical characterizations of the pumice and Portland cement were detected. Water demand, setting time, and volume expansion of paste samples with standard cement tests were determined. The XRD and TGA results prove that the pumice–containing cement displays a high hydration degree on the 90th day and will continue to hydrate. Furthermore, on the 90th day, the chemically bound water content in 10P paste is the same as that in Portland cement. Moreover, SEM images reveal that the usage of pumice results in a much denser microstructure as the hydration age increases. The results showed that pumice has lower pozzolanic activity in the early period and yet the compressive strength increases with time.

1. Introductıon

Mineral additives, which find use in the cement and concrete industry, have become an indispensable product as the preferred basic supplementary cementitious materials. They hold significant economic and ecological advantages and contribute to the development of properties such as the strength and durability of concrete. Therefore, to improve these properties of cement and concrete, natural pozzolanic materials (e.g., zeolite, diatomite trass), industrial wastes (e.g., silica fume, fly ash, ground granulated blast furnace slag), or heat-treated mineral additives (e.g., methacholine, rice husk ash) are used extensively [1–11].

Pumice is among the rich resources of Turkey, and it is estimated that 68% of the world's pumice reserves are in Turkey [12]. Using pumice has been studied in many applications such as aggregates for lightweight concretes [13–15]; a filler of self–compacting concrete [16,17]; partial replacement of cement and concretes [18,19]; as well as other applications [20–23].

Pumice is a silicate-based, porous and spongy–looking rock that can be found in various colors from dirty white to gray, red and brown to black, formed by the sudden cooling of the gases in the hot magma as a result of volcanic activities. Pumice is available in two types, i.e., acidic and basic. The most used is acidic pumice, and its color is clear. Its hardness in the Mohs scale varies between 5 and 6, and its density varies between 0.5 and 2 g/cm^3. In its chemical composition, besides silicon, aluminum, iron, calcium, magnesium, sodium, and potassium, there are also trace amounts of titanium and sulfur [24,25]. Using pumice as an additive to cement not only improves durability parameters and decreases the amount of cement but also causes changes in the mineralogical and molecular structures. All these are due to the fact that cement and pozzolans are materials with hydration reactions that are intricate, and no method has been proposed that can detect chemical reactions occurring in the structures of these materials. For this reason, in this study, X-ray Diffraction (XRD), Differential Thermal and Thermogravimetric Analysis (DTA/TGA), Fourier Transforms Infrared Spectroscopy (FT–IR), and Scanning Electron Microscopy (SEM) analyses were used to investigate complex hydration reactions. Furthermore, mechanical, physical, and chemical features belonging to PC, pumice–substituted cement mortar, and paste samples substituted cement were studied through basic cement evaluations.

* Corresponding author.
E-mail address: yilmazkocak@duzce.edu.tr (Y. Kocak).

https://doi.org/10.1016/j.conbuildmat.2022.127528
Received 15 March 2022; Received in revised form 11 April 2022; Accepted 12 April 2022
Available online 19 April 2022
0950-0618/

Table 1
Composition of mixtures prepared in this study.

Kod	Cement, g	Cement, %	Pumice, g	Pumice, %	Standart sand, g	w/c
R	450	100	0	0	1350	0.5
10P	405	90	45	10		
20P	360	80	90	20		

Table 2
Chemical and physical characteristics of PC and pumice.

Materials		PC	Pumice
Chemical composition, wt.%	SiO_2 (S)	20.36	56.32
	Al_2O_3 (A)	4.6	16.51
	Fe_2O_3 (F)	2.56	3.93
	CaO	62.57	4.84
	MgO	1.53	1.87
	SO_3	3.32	0.23
	Na_2O	0.26	5.18
	K_2O	0.66	5.09
	Loss on ignition	2.38	2.65
	Cl^-	0.018	0.010
	Free CaO	1.78	–
	S + A + F	–	76.76
Physical characteristics	Specific gravity, g/cm^3	3.18	2.70
	Blaine, cm^2/g	3822	2645
	Retained on 45–μm, %	3.2	40.5
	Retained on 90–μm, %	0	7.8

2. Materıals and methods

2.1. Materials

The main materials of the study were CEM I 42.5 R Portland cement, pumice, standard aggregate, and water. The Portland cement (PC) was produced by Eskisehir Cement Plant. Pumice was supplied by the Belmas Company (Isparta–Turkey). In the composition of mortars, the sand, which is standard CEN type conforming to TS EN 196–1 [26], along with regular tap water belonging to Eskisehir, a province of Turkey, was utilized.

2.2. Methods

Chemical analyses in equivalent oxides of PC and pumice were performed by ARL 9900 Intellipower X-ray Analyzer. The Rikagu SmartLab XRD was utilized, and Cu Kα (λ = 1.54 A°) radiation was used to detect the mineralogical properties. FT–IR analyses were conducted using Shimadzu IRPrestige 21. DTA/TGA curves were determined using a simultaneous thermal analysis instrument (Shimadzu DTG 60H–DSC 60) under nitrogen atmosphere by heating from 20 °C to 1000 °C with 10 °C/min steps. An FEI Quanta FEG 250 model was used for the analysis of the microstructure of paste samples. Surface areas by Toni Technik 7202 Blaine, specific gravity by Quanta Chrome MVP–1, and fineness determination by Hosokawa 200 LSN (air jet sieve) were determined.

In this study, PC was used for preparing reference paste and mortar, which was named R. The pumice was grounded in a ball mill for 30 min, and, it was added as a partial substitution for PC at a weight level of 10% and 20%, respectively, demonstrated as 10P and 20P. The prepared samples are shown in Table 1.

Paste specimens were prepared by using the laboratory-type mixer in accordance with TS EN 196–1 [26]. Water demands, volume expansion, and setting times of paste specimens were verified conforming to TS EN 196–3 [27]. Water demands and setting times were determined with Vicat's needle apparatus on the paste specimens. XRD, FTIR, DTA/TGA, and SEM paste samples were created by using a constant water-cement ration (W/C) of 0.35 based on these findings. The pastes were grounded on the 2nd, 7th, 28th, and 90th days.

Mortars prepared to determine the compressive strengths were placed into three–segmented rectangular prism molds of size 40x40x160 mm in compliance with TS EN 196–1. The mortar was placed in a mold shaking device and shaken considering the principles specified in the standard. These produced samples were secured in a laboratory environment at 90% humidity and 20 ± 1 °C temperature for 24 h. The samples were taken from the molds at the end of this time and placed in a curing pool at a temperature of 20 ± 1 °C until the test days. Specimens were gathered from the pool on the 2nd, 7th, 28th, and 90th days, and were duly broken in half. The compressive strengths of these six samples, which were later broken in the middle, were determined according to TS EN 196–1 [26], averaged, and calculated as the final compressive strength.

3. Experımental results and dıscussıon

3.1. Chemical and physical analysis

The chemical and physical characteristics of PC and pumice are on display in Table 2. SEM/EDS images were given in Fig. 1.

By comparing the chemical compositions of materials, the PC comprises CaO, SiO_2, Al_2O_3, SO_3, Fe_2O_3, MgO, and traces of K_2O, Na_2O, respectively. The main components of pumice are SiO_2 and AlO_2, respectively. Also, the pumice contains K_2O, Na_2O, CaO, Fe_2O_3, and MgO and traces of SO_3. According to chemical composition, it is detectable that the mass fractions of S + A + F are 76.76% for pumice (Table 2), and it complies with the stated requirements (>70%) for a natural pozzolan [28]. The specific weights of the PC and pumice are 3.18 and 2.70 g/cm^3. Their specific surfaces (Blaine) are 3822 and 2645 cm^2/g, respectively. Furthermore, residue on 45 and 90 μm sieve of the PC and pumice are 3.2–0%, and 40.5–7.8%, respectively. As seen from Fig. 1(a and b), cement and pumice have porous structures comprising rough and accidental micropores. Moreover, it is possible to see its amorphous structure (glassy form), non–uniform plate shape, and irregular morphology of the pumice from its microstructure image [12,23]. Cement and pumice are mostly made up of the elements Ca and Si, according to EDS analysis (Fig. 1a and b).

3.2. Mineralogical structure

XRD analyses were performed to detect the mineralogical structures of PC and pumice. The XRD patterns of the materials are given in Fig. 2.

The main components of PC, regarding the XRD pattern, are C_3S ($3CaOSiO_3$), C_2S ($2CaOSiO_3$), C_3A ($3CaO.Al_2O_3$), and C_4AF ($4CaO.Al_2O_3\,3.Fe_2O_3$) (Fig. 2-a). As observed from the patterns of pumice, it has an amorphous structure comprising amorphous quartz (SiO_2) substance at 2θ = 20–32° and some crystalline phases as albite ($NaAlSi_3O_8$), calcite ($CaCO_3$), anorthite ($CaAl_2Si_2O_8$) [18,29] (Fig. 2-b). The components observed in the crystalline structure of PC and pumice with XRF and XRD analyses are compatible.

3.3. FT–IR analysis

The surface structures of the molecules of PC and Pumice were determined by FT–IR studies, and the FT–IR diagram of the materials is displayed in Fig. 3.

In FT–IR spectroscopy of PC, peaks of vibration are observed at wave numbers of 507, 735, 902, 1124, 1413, and 1385 cm^{-1} (Fig. 3). The Al–O bond appearing along with Si-O may be responsible for the major FT–IR band at 507 cm^{-1}. The band that appeared at 902 cm^{-1} is affiliated with Si–O bonds in cage structures. Bands at 735 and 1124 cm^{-1} in the existence of Sulfur–Oxygen (S–O) bonds, showing the plaster in PC. Bands at around 1413 cm^{-1} are associated with CO_3^{-2} (Fig. 3) [30–32].

The FT–IR spectrum data of pumice are 457, 548, 708, 997, and 1424 cm^{-1}, as Fig. 6 displays. In the FT–IR spectrum, the strong band at

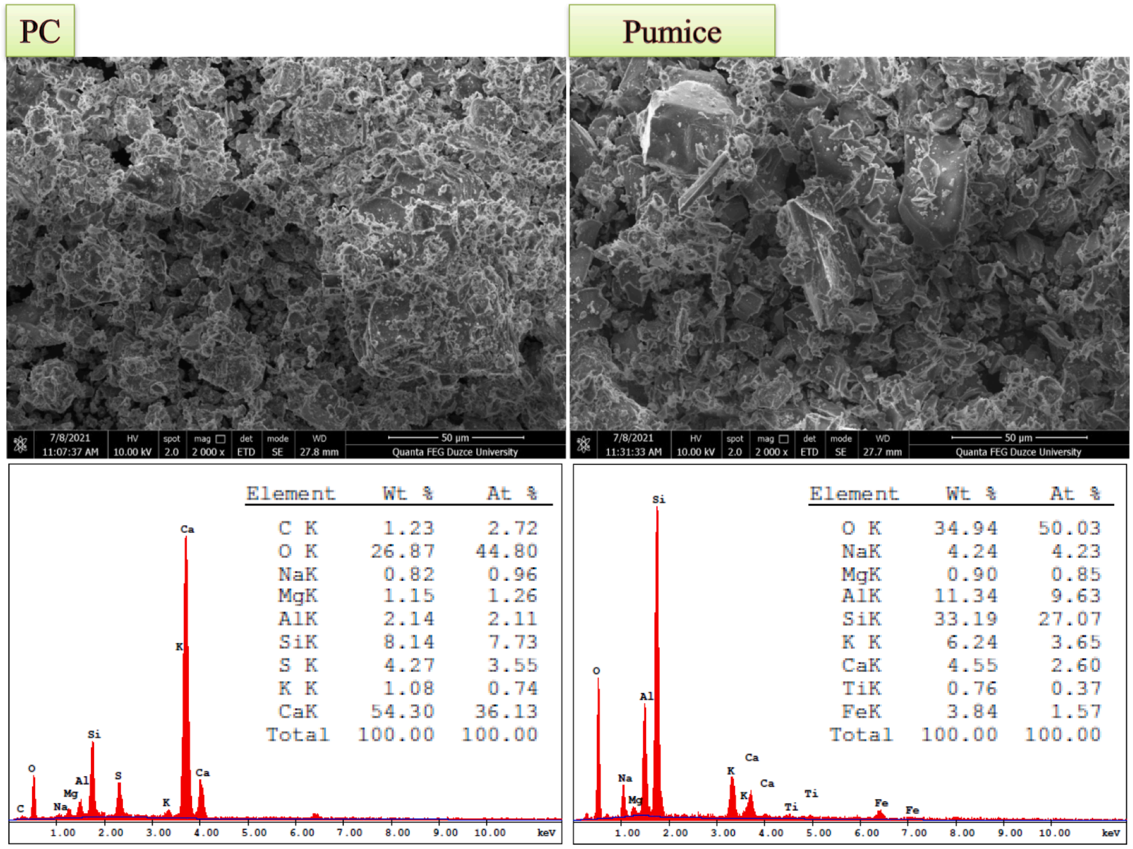

Fig. 1. The images of PC and pumice by SEM and EDS area.

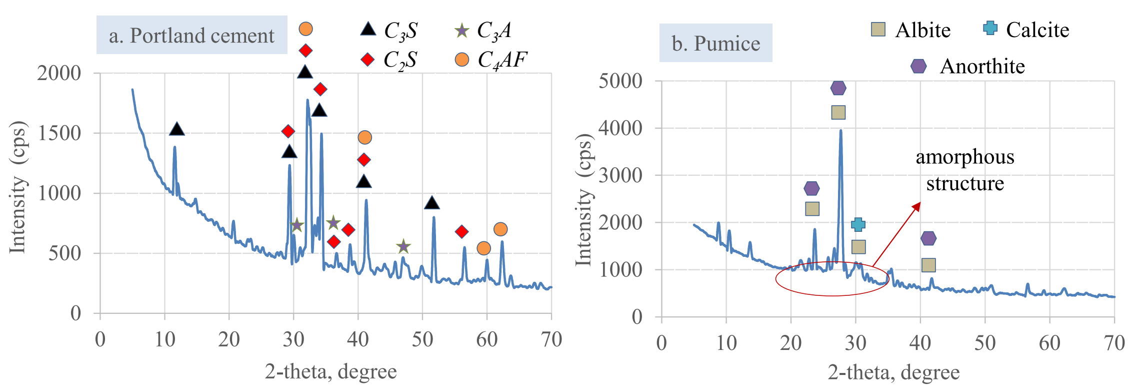

Fig. 2. XRD patterns of PC and pumice.

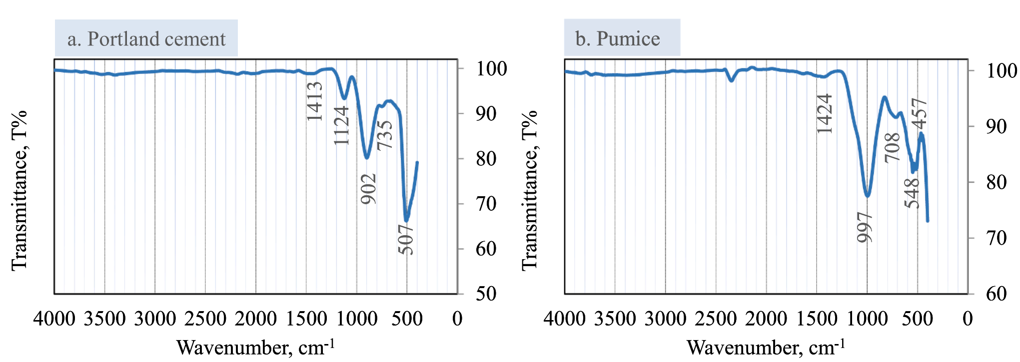

Fig. 3. FT–IR diagram of PC and pumice.

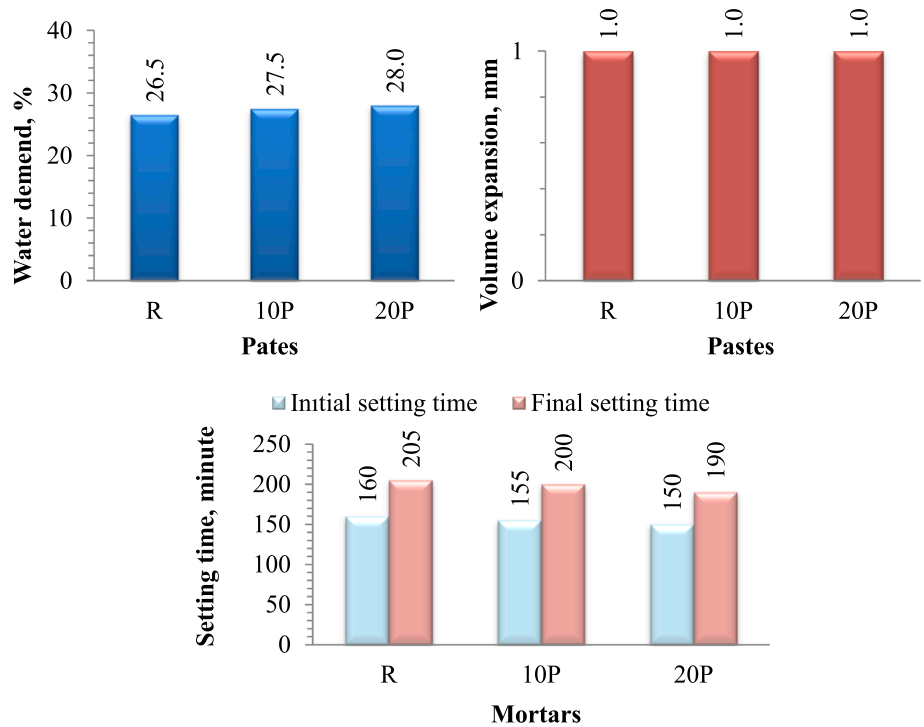

Fig. 4. Water demand, volume expansion, and setting time of pastes.

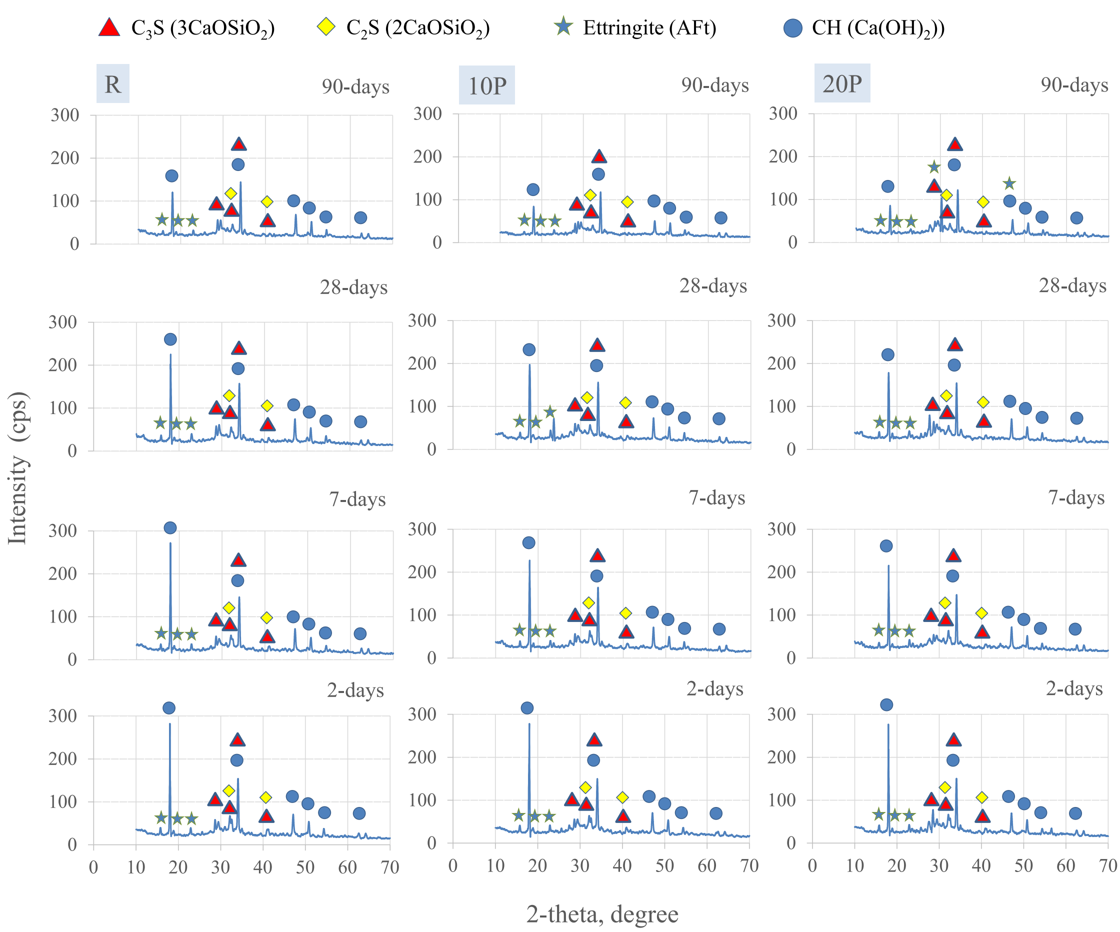

Fig. 5. XRD patterns of pastes.

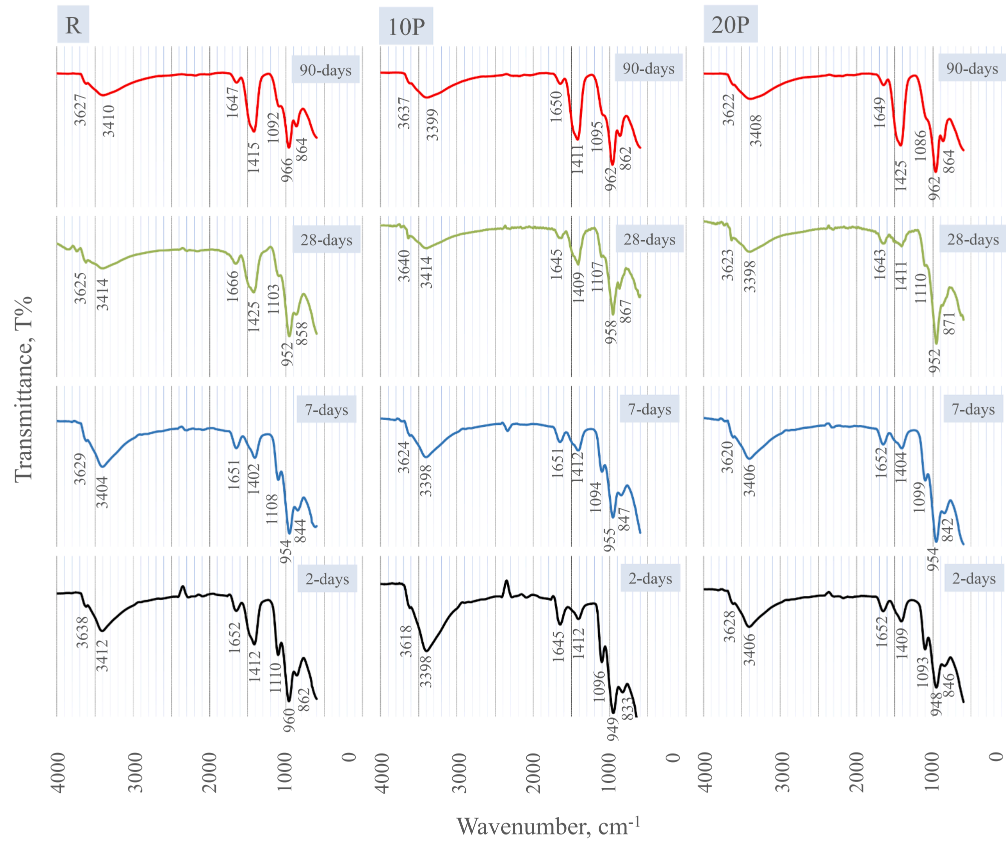

Fig. 6. FT–IR diagram of pastes.

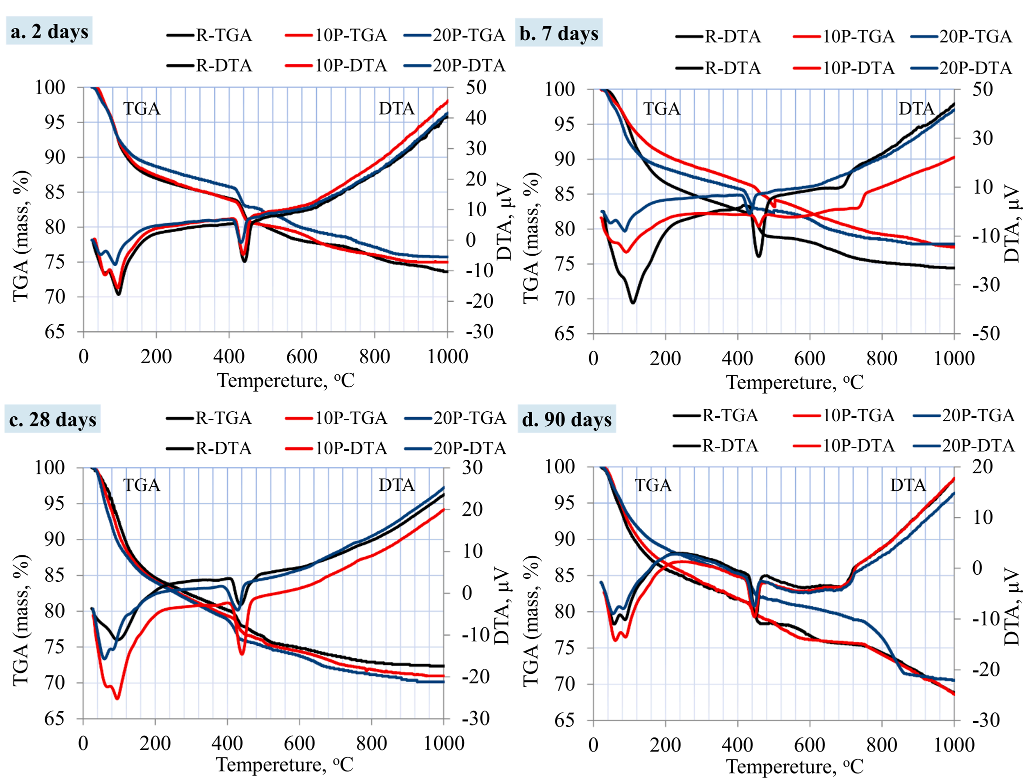

Fig. 7. DTA/TGA patterns of pastes.

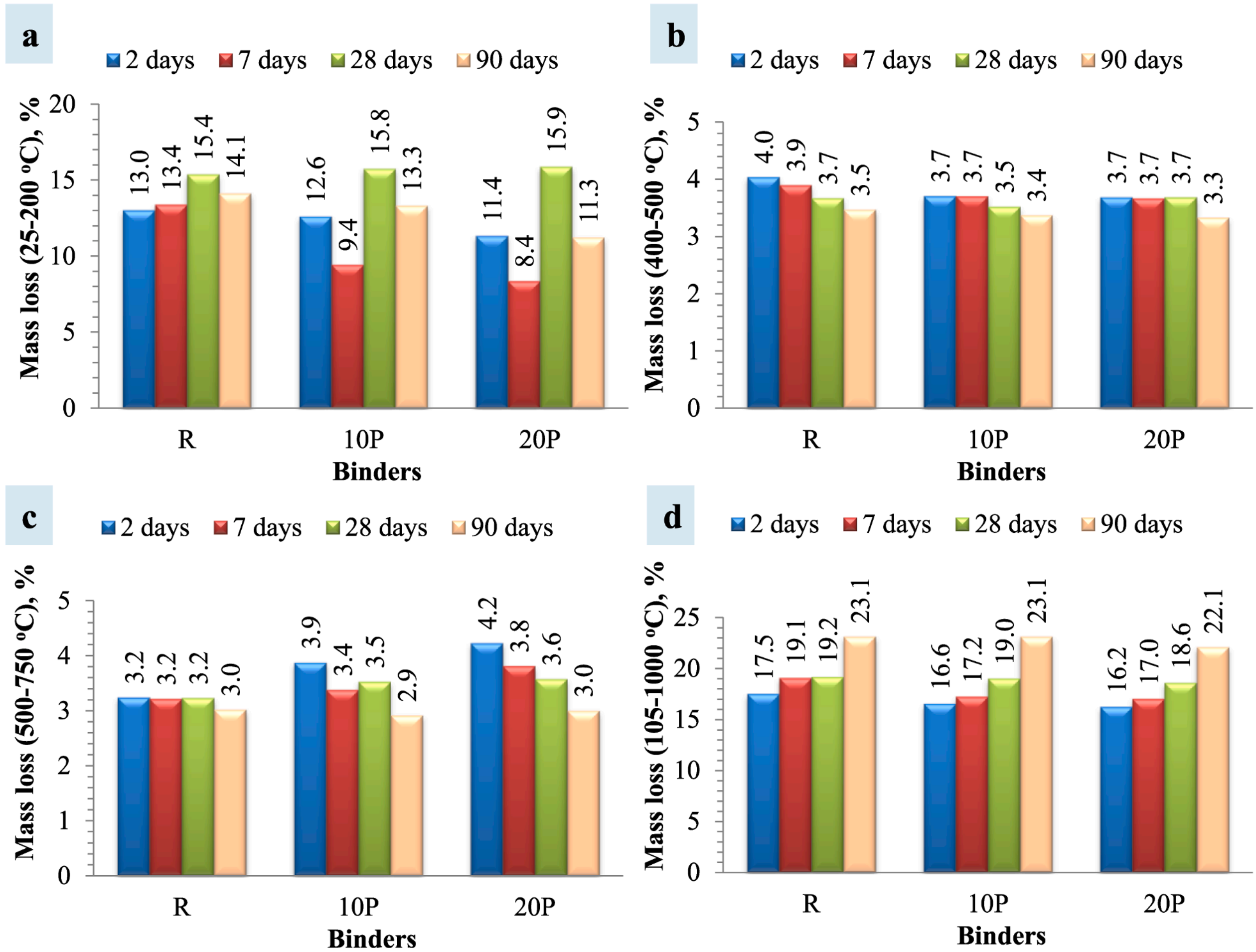

Fig. 8. Result of TGA of pastes cured for different hydration days.

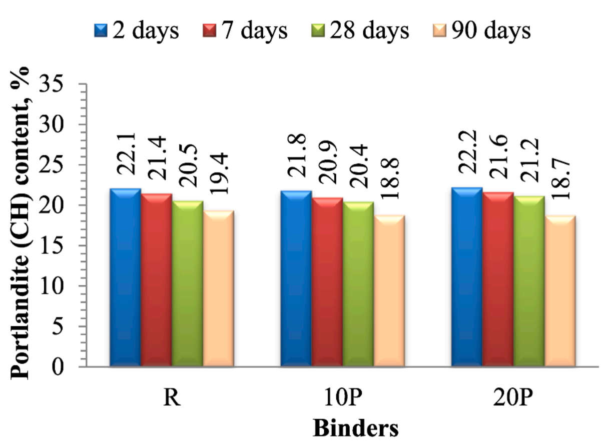

Fig. 9. The whole content of CH.

997 cm^{-1} is attributed to Si–O–(Si, Al) bonds. Weaker bands in the region 708 cm^{-1} are associated with Si–O bending strength vibrations of amorphous quartz. The band at 1424 cm^{-1} is attributed to CH bonds. The Al–O bond appearing along with Si–O may be responsible for bands at 435 and 542 cm^{-1} [12,29,33]. Results were confirmed by the XRF and XRD results.

3.4. Water demand, volume expansion and setting time

The water demand, volume expansion, and the time necessary for paste specimens to set are shown in Fig. 2.

Water demand varies with regard to the porosity values, Blaine, and chemical composition of PC and pumice. Compared with pure paste, the water demand of the 10P and 20P coded paste specimens was decreased by 18% and 34%, respectively (Fig. 4-a). Excessive levels of free lime, magnesia, and calcium sulfate in the cement may cause expansions, which can cause cracking and damage to the concrete. The volume expansion was detected using Le Chatelier's technique. As seen from Fig. 4-b, values of volume expansion were 1 mm. Therefore, each value was less than 10 mm, which corresponds to the TS EN 1963- cutoff value [27]. It is observed that the addition of pumice decreases both initial and final setting times of pastes, compared with pure paste (Fig. 4). Compared to pure paste, the initial setting time of the 10P and 20P coded paste specimens was decreased by 3% and 6%, and the final setting time was decreased by 2% and 5%, respectively (Fig. 4c). Regarding the setting times, it was determined that all pastes are above the minimum initial setting time, which is 60 min for 42.5 R type cement in the standard [34].

3.5. XRD analysis of the cement pastes

XRD patterns of the pastes on the 2nd, 7th, 28th, and 90th days are given in Fig. 5.

Because of its amorphous structure, in the XRD spectra of the

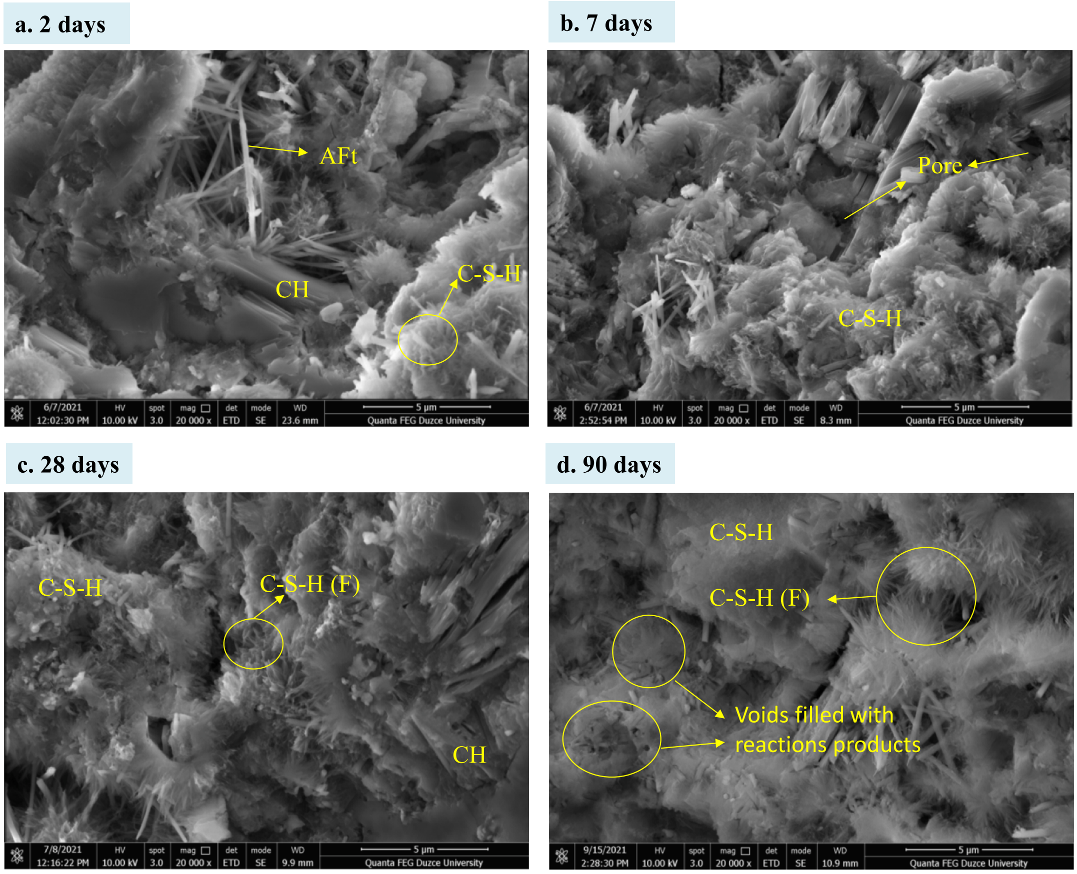

Fig. 10. SEM images of R coded pastes.

hydrated calcium silicate gel, there are no diffraction bonds, and XRD spectra cannot reveal the amorphous SiO2 content of Pumice either. Crystalline phases in the hydration products of R, 10P, and 10D pastes are mainly CH (portlandite), unhydrated calcium silicate (C_3S or C_2S), and ettringite (AFt). CH, the main hydration product in the three pastes, represents the cement hydration degree. Fig. 5 reveals that the characteristic peak of CH in R, 10P, and 20P paste samples on the 2nd day has almost the same affinity. On the 7th, 28th, and 90th days, however, the intensities of CH diffraction bands of 10P and 20P compared with R is weaker, so the amount of CH in 10P and 20P is lesser than R. The reason for this is that the pumice's pozzolanic reaction often consumes the coarse plate-like CH crystals to form C–S–H gel in cement-based pastes. Thus, lower CH concentration improves the mechanical characteristics of 10P and 20P [35,36,37].

3.6. FT–IR analysis of the cement pastes

The FT–IR spectra of the pastes on the 2nd, 7th, 28th, and 90th days of hydration are given in Fig. 6.

As most paste hydration products are amorphous C–S–H, FT–IR is a frequently utilized tool that enables measuring the hydration products and their relative quantities through stimulation of their usual wave numbers and transmittance [37]. The predominant mid-FT–IR bands at 949–960 cm^{-1} in hydrated pastes are attributable to antisymmetric Si–O stretching vibrations and in-plane Si–O bending vibrations in SiO4 tetrahedra, which indicate C–S–H formation, respectively. The peak that appeared at 1080–1110 cm^{-1} can be attributed to Si–O due to the formation of ettringite. The C–O stretching at around 1400–1419 cm^{-1} and a weak shoulder band at 823–867 cm^{-1} are associated with antisymmetric stretching and out–of–plane bending modes of CO_3^{2-} ions, which is the product resulting from carbonation. Bands at 3379–3394 cm^{-1} and 1640–1652 cm^{-1} can be attributed to O–H stretching and molecular water, respectively. The wide absorption band at wave number 2800–3700 cm^{-1} depicts the presence of $CaCO_3$, which displays a diminishing tendency as hydration progresses. The bands at 3583–3634 cm^{-1} can be attributed O–H, which are associated with the formation of CH appears (Fig. 6) [33,37–40]. This result complies with the XRD analysis results.

3.7. Thermal analysis of the cement pastes

Fig. 7 displays the outcomes of DTA/TGA analysis of the pastes during the 2nd, 7th, 28th, and 90th days after hydration.

Utilization of cement hydrated products such as C–S–H and CH has been investigated using DTA/TGA analyses (Fig. 7). Different endothermic peaks can be seen in the DTA curves, and a significant weight loss may occur in the TG curves. The endothermic peak in the temperature range 25–200 °C is due to the vaporization of free water and dehydration of C–S–H and AFt. The endothermic peak around 400–500 °C is associated with dehydration of CH. Due to the decomposition of $CaCO_3$ from the carbonization of CH while preparing the samples, the peak around 700 °C' occurs [41]. In addition, the chemically bound water content, which is the dehydration of cement hydration products, including C–S–H gel, portlandite, and other hydrated products, is determined by weight loss between 105 °C and 1000 °C [42,43].

Equation (1) can enable computing the overall CH content in pastes by using the mass of CH dehydration and $CaCO_3$ decomposition:

$$CH(\%) = x^* \frac{74}{18} + y^* \frac{74}{44} \tag{1}$$

In equation (1), x represents the weight losses due to dehydration of

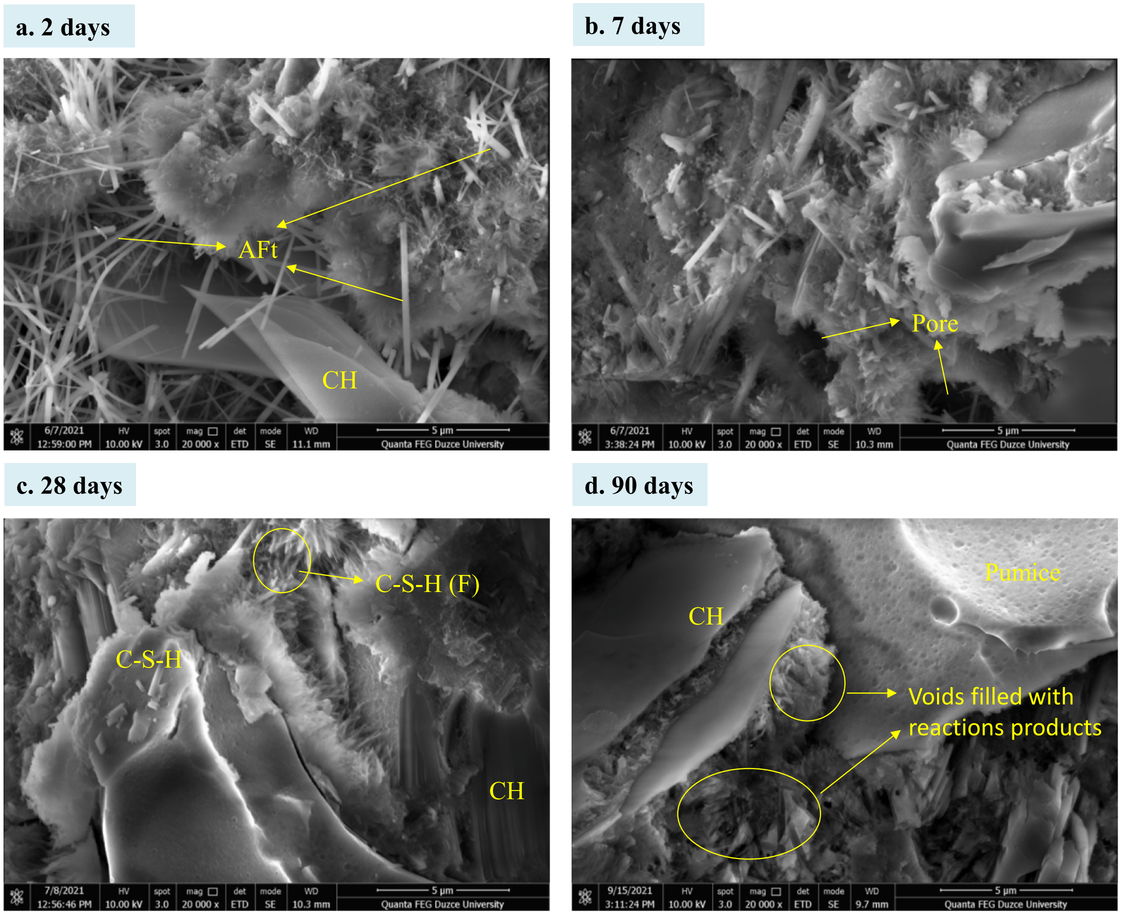

Fig. 11. SEM images of 10P coded pastes.

CH, and y represents the breakdown of $CaCO_3$. The molecular weights of CH, H_2O, and CO_2 are 74, 18, and 44, respectively [42,43].

The amounts of free water, AFt, and C–S–H on the 2nd, 7th, 28th, and 90th days calculated by the TGA analysis of the R paste samples are 13.0–13.4–15.4–14.1%; that in 10P are 12.6–9.4–15.8–13.3%; in 20P are 11.4–8.4–15.9–11.3, respectively (Fig. 8a). In Fig. 8 (b, c), weight losses resulting from dehydration of CH and disintegration of $CaCO_3$ in paste samples on the 2nd, 7th, 28th, and 90th days are given. The content of CH on the 2nd, 7th, 28th, and 90th days in R paste samples calculated by the equation are 22.1–21.4–20.5–19.3%; that in 10P are 21.8–20.9–20.4–18.8%, and in 20P are 22.2–21.6–21.2–18.7%, respectively (Fig. 9). With the addition of 10% and 20% pumice, the content of CH is reduced gradually. The content of chemically bound water on the 2nd, 7th, 28th, and 90th days in R paste samples calculated by the equation are 17.5–19.1–19.2–23.1%; that in 10P are 16.6–17.2–19.0–23.1%, and in 20P are 16.2–17.0–18.6–22.1%, respectively (Fig. 8). Results indicate that the highest percentages of total chemically bound water on the 2nd, 7th, and 28th days are obtained for the mixture with R paste. However, on the 90th day of hydration, the 10P paste was reached the same percentage of chemically bound water as the reference paste. This may indicate that more hydration products are formed in the pumice–substituted paste and have a more compact structure later age.

3.8. Microstructure analysis of the cement pastes

SEM images of R, 10P, and 20P coded pastes hydrated for the 2nd, 7th, 28th, and 90th days are given in Figs. 10, 11, and 12, respectively.

According to the early hydration of Portland paste, Fig. 10(a, b) reveals that the radiating fibers of C–S–H surrounded the clinker grains. This fibrillar morphology of C–S–H rich in lime seen in Fig. 8a–b shows a comparatively high porosity when compared to pozzolan-added pastes with crumpled C–S–H foils. Elongated needle-shaped AFt (ettringite) crystals were found in gaps and cracks, while portlandite crystals emerged as stacked massive morphology (Fig. 10a). On the 7th day of hydration, a reticular network morphology is clear with interaction and bridging between grains (Fig. 10b). In the paste, the amorphous gel, which suffuses the whole gap among particles, provides the building absolute stability, takes on the dominant role on the 28th and 90th days, and the classic fusion of layered CH with Type III gel becomes observable (Fig. 10c, d) [19,44,45].

At early ages, the central structure of PC–pumice mixture is slightly crystallized foils of C–S–H phase in a pattern pertaining to C–S–H Type I (Fig. 11a, 12a). AFt phase appeared as stubby rods, and thin flakes of aluminate hydrates filled the porous areas in the paste (Fig. 11a). 10P and 20P coded pastes exhibited a dense structure at 7 hydration days, with most of the spaces between pumice and matrix filled with the formation of acicular features indicative of Type 1C–S–H (Fig. 11b, 12b). From the 7th to the 28th and 90th days, a slight increase in hydration products and densification in the C–S–H structure were observed (Fig. 11c-d, 12c-d). AFt, igneous crystals were not observed at this hydration age. This is due to the conversion of AFt to AFm (mono sulfoaluminate) after the depletion of sulfate (Fig. 11c-d, 12c-d). Furthermore, after the 7th day of hydration, it was observed that all hydration products overlap and intertwine, resulting in the emergence of a progressively higher-strength, dense structure (Fig. 11c-d, 12c-d). When the microstructure results of the pumice-replaced pastes are evaluated, it can be expected that there is a good agreement between the pore structure of the hardened cementitious pastes and the mechanical properties of mortars [19,44,45].

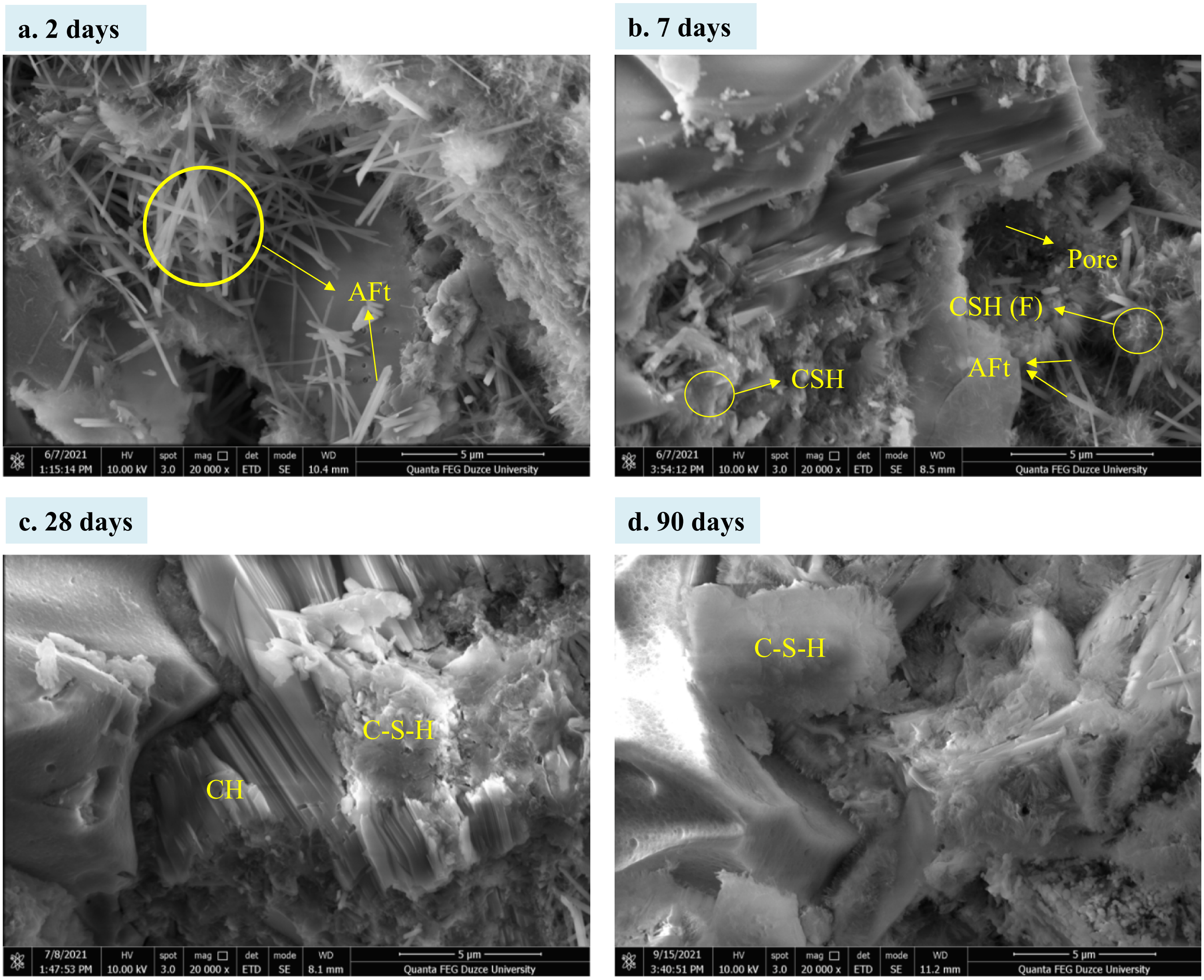

Fig. 12. SEM images of 20P coded pastes.

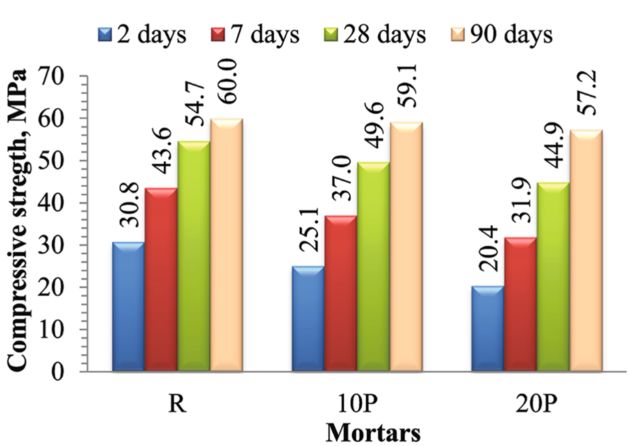

Fig. 13. Compressive strength of mortars.

3.9. *Compressive strength*

Compressive strength tests were performed on the mortar specimens in accordance with TS–EN 196–1 [26]. The 2nd, 7th, 28th, and 90th days compressive strength experiments results of mortar specimens were given in Fig. 13.

The compressive strength of the mortar samples depends on the type of hydration time, replacement rate, particle size, and specific surface areas. The compressive strength of the produced mortar specimens reduced by 18.5% after the 2nd day; 15.1% after the 7th day; 9.2% after the 28th day; and 1.4% after the 90th day, in comparison to the mortar samples PC produced. After adding 20% pumice to PC, the compressive strength of the produced mortar specimens diminished by 33.7% after the 2nd day; 26.9% after the 7th day; 17.8% after the 28th day; and 4.5% after the 90th day, in comparison to the mortar samples PC produced. The data of the conducted test revealed that the compressive strength obtained for each pumice replacement rate is lower than the value obtained for PC mortar. However, a constant and rapid increase can be observed in the compressive strength of mortars containing pumice, notably in the following ages. The pumice consumes more CH to form C–S–H gel at a later age (Fig. 9), resulting in a microstructure that is denser in comparison to Portland paste (Figs. 10-12). Furthermore, the chemically bound water content and its compressive strength on the 90th day are the same as those in Portland paste and mortar. Furthermore, the values of compressive strength on the 28th day for all mortar samples with 10% and 20% pumice were found to be higher than the minimum value of 42.5 MPa, which can help save up to 20% on Portland cement (Fig. 13).

4. Conclusıons

In this study, XRD, SEM, FT–IR, and DTA/TGA methods were employed to examine the hydration mechanisms and mechanical properties of pumice substituted cementitious binder on the 2nd, 7th, 28th, and 90th days. According to the findings obtained in this study, the following conclusions can be reached:

- Pumice–added pastes require a litle more mixing water than pure paste.
- The volume expansion values of each paste emerged to be less than 10 mm, indicating that the expansions were less than the maximum value TS EN 196–3 proposed.
- Regarding the time, it was determined that all pastes are above the minimum initial setting time, which is 60 min for 42.5 R type cement in the standard.
- The XRD and TGA results prove that the pumice–containing cement reveals a high hydration degree at 90th days and will continue to hydrate. Furthermore, on the 90th day, the chemically bound water content in 10P paste is the same as that in Portland cement.
- SEM images indicated that their hydration products were mainly AFt, CH, and C–S–H gels and a much denser microstructure of pastes with pumice as the hydration age increases.
- The improvement effect on the compressive strength of pumice appears mainly on the 90th day. While mortars with pumice show a continuous increase in compressive strength particularly on the 28th and 90th days, they exhibit a significant loss of compressive strength on the 2nd and 7th days. The results showed that pumice has lower pozzolanic activity at early ages but at later age increases. This is leading to an increase in compressive strength. Furthermore, the compressive strength values at the end of the 28th day for all mortar samples with 10% and 20% pumice were measured above the minimum value of 42.5 MPa, which will save up to 20% of Portland cement.

Declaration of Competing Interest

The authors indicate that they have no known personal relationships or competing financial interests that could have appeared to influence the work reported in the manuscript.

Acknowledgments

This study was supported by Düzce University Research Fund (Project Code No: 2021.06.08.1190). In addition, the authors would like to thank the Eskişehir CIMSA cement factory managers and employees for their invaluable contributions to this study.

References

[1] A.R.L. Kushnir, M.J. Heap, L. Griffiths, F.B. Wadsworth, A. Langella, P. Baud, T. Reuschlé, J.E. Kendrick, J.E.P. Utley, The fire resistance of high-strength concrete containing natural zeolites, Cement and Concrete Composites 116 (2021) 103897, https://doi.org/10.1016/j.cemconcomp.2020.103897.
[2] C. Karakurt, İ.B. Topçu, Effect of blended cements produced with natural zeolite and industrial by–products on alkali–silica reaction and sulfate resistance of concrete, Construction and Building Materials 25 (2011) 1789–1795.
[3] Y. Kocak, E. Tascı, U. Kaya, The effect of using natural zeolite on the properties and hydration characteristics of blended cements, Construction and Building Materials 47 (2013) 720–727.
[4] H. Gerengi, Y. Kocak, A. Jażdżewska, et al., Electrochemical investigations on the corrosion behaviour of reinforcing steel in diatomite– and zeolite–containing concrete exposed to sulphuric acid, Construction and Building Materials 49 (2013) 471–477.
[5] M. Sun, C. Zou, D. Xin, Pore structure evolution mechanism of cement mortar containing diatomite subjected to freeze-thaw cycles by multifractal analysis, Cement and Concrete Composites 114 (2020) 103731, https://doi.org/10.1016/j.cemconcomp.2020.103731.
[6] Y. Koçak, The effects of super plasticizer and trass on the cement hydration, Pamukkale University Journal of Engineering Sciences 23 (3) (2017) 184–192.
[7] A. Joshaghani, The effect of trass and fly ash in minimizing alkali-carbonate reaction in concrete, Construction and Building Materials 150 (2017) 583–590.
[8] G. Adil, J.T. Kevern, D. Mann, Influence of silica fume on mechanical and durability of pervious concrete, Construction and Building Materials 247 (2020) 118453, https://doi.org/10.1016/j.conbuildmat.2020.118453.
[9] Y.J. Lee, H.G. Kim, K.H. Kim, Effect of Ground Granulated Blast Furnace Slag Replacement Ratio on Structural Performance of Precast Concrete Beams, Materials 14 (23) (2021) 7159.
[10] M.Á. Sanjuán, E. Estévez, C. Argiz, D. del Barrio, Effect of curing time on granulated blast-furnace slag cement mortars carbonation, Cement and Concrete Composites 90 (2018) 257–265.
[11] A. Hasanbeigi, L. Price, E. Lin, Emerging energy–efficiency and CO_2 emission–reduction technologies for cement and concrete production: Atechnical review, Renewable and Sustainable Energy Reviews 16 (8) (2012) 6220–6238.
[12] A. Yucel, T. Efe, M. Onal, et al., Mineralogical and chemical characterization of acidic pumices outcrop North of Lake Van, In IOP Conference Series: Earth and Environmental Science (2016, October) 052019). IOP Publishing.
[13] R.B. Karthika, V. Vidyapriya, K.N., et al., Experimental study on lightweight concrete using pumice aggregate, Materials Today: Proceedings 43 (2021) 1606–1613.
[14] M. Kurt, M.S. Gül, R. Gül, et al., The effect of pumice powder on the self-compactability of pumice aggregate lightweight concrete, Construction and Building Materials 103 (2016) 36–46.
[15] Malik Shafiq, Fasih Khan, Yasir Badrashi, Fayaz Khan, Muhammad Fahim, Asim Abbas, Waqas Adil, Evaluation of Mechanical Properties of Lightweight Concrete with Pumice Aggregate, Advances in Science and Technology Research Journal 15 (2) (2021) 30–38.
[16] M.F. Granata, Pumice powder as filler of self-compacting concrete, Construction and Building Materials 96 (2015) 581–590.
[17] Mahya Askarian, Siavash Fakhretaha Aval, Alireza Joshaghani, A comprehensive experimental study on the performance of pumice powder in self-compacting concrete (SCC), Journal of Sustainable Cement-Based Materials 7 (6) (2018) 340–356.
[18] K. Cabrera-Luna, E.E. Maldonado-Bandala, D. Nieves-Mendoza, P. Castro-Borges, P. Perez-Cortes, J.I. Escalante García, Supersulfated cements based on pumice with quicklime, anhydrite and hemihydrate: Characterization and environmental impact, Cement and Concrete Composites 124 (2021) 104236, https://doi.org/10.1016/j.cemconcomp.2021.104236.
[19] Kaizhi Liu, Rui Yu, Zhonghe Shui, Xiaosheng Li, Xuan Ling, Wenhao He, Shuangqin Yi, Shuo Wu, Effects of pumice-based porous material on hydration characteristics and persistent shrinkage of ultra-high performance concrete (UHPC), Materials 12 (1) (2019) 11, https://doi.org/10.3390/ma12010011.
[20] M.S. Amin, F.S. Hashem, S.M.A. El-Gamal, Utilization of OPC-Pumice composites for efficient heavy metals removal, Journal of Taibah University for Science 12 (6) (2018) 765–773.
[21] M. Taherishargh, I.V. Belova, G.E. Murch, T. Fiedler, Pumice/aluminium syntactic foam, Materials Science and Engineering: A 635 (2015) 102–108.
[22] M.E. Stringer, Separation of pumice from soil mixtures, Soils and Foundations 59 (4) (2019) 1073–1084.
[23] Ahmet Sarı, Gökhan Hekimoğlu, V.V. Tyagi, R.K. Sharma, Evaluation of pumice for development of low-cost and energy-efficient composite phase change materials and lab-scale thermoregulation performances of its cementitious plasters, Energy 207 (2020) 118242, https://doi.org/10.1016/j.energy.2020.118242.
[24] G. Eroğlu, M., Şahiner, Dünyada Ve Türkiye'de Pomza, Maden Tetkik Ve Arama Genel Müdürlüğü Fizibilite Etütleri Daire Başkanlığı, (2020) 1–32. in Turkey.
[25] N. Elmastaş, Türkiye Ekonomisi İçin Önemi Giderek Artan Bir Maden: Pomza (Sünger Taşi), Journal of International Social Research 5 (23) (2012) 197–206, in Turkey.
[26] TS EN 196–1, Methods of testing cement–Part 1: Determination of strength. Turkish Standards 2002, Ankara–Turkey.
[27] TS EN 196-3, Methods of testing cement–Part 3: Determination of setting time and soundness, Turkish Standards 2017, Ankara-Turkey.
[28] TS 25, Natural pozzolan (Trass) for use in cement and concrete - Definitions, requirements and conformity criteria, Turkish Standards 2015. Ankara-Turkey.
[29] Mustafa Sarıdemir, Metehan Bulut, Effects of ground basaltic pumice and high temperatures on the properties of HSMs, Journal of Building, Engineering 41 (2021) 102772, https://doi.org/10.1016/j.jobe.2021.102772.
[30] C.E.M. Gomes, O.P. Ferreira, Analyses of microstructural proporties of va/veova copolymer modified cement pastes, Polimeros: Ciencia E Tecnologia 15 (3) (2005) 193–198.
[31] Carlos Eduardo Marmorato Gomes, Osny Pellegrino Ferreira, Mauro Roberto Fernandes, Influence of vinyl acetate–versatic vinylester copolymer on the microstructural characteristics of cement pastes, Material Research 8 (1) (2005) 51–56.
[32] A. Govin, A. Peschard, R. Guyonnet, Modification of cement hydration at early ages by natural and heated wood, Cement & Concrete Composites 28 (1) (2006) 12–20.
[33] M.N. Sepehr, A. Amrane, K.A. Karimaian, et al., Potential of waste pumice and surface modified pumice for hexavalent chromium removal: characterization, equilibrium, thermodynamic and kinetic study, Journal of the Taiwan Institute of Chemical Engineers 45 (2) (2014) 635–647.
[34] TS EN 197–1. Cement– Part 1: Compositions and conformity criteria for common cements. Turkish Standards 2002. Ankara–Turkey.

[35] A. Schöler, B. Lothenbach, F. Winnefeld, M. Zajac, Hydration of quaternary Portland cement blends containing blast-furnace slag, siliceous fly ash and limestone powder, Cement and Concrete Composites 55 (2015) 374–382.
[36] Yasong Zhao, Jianming Gao, Zhenhai Xu, Shujun Li, Xu Luo, Gaofeng Chen, Long-term hydration and microstructure evolution of blended cement containing ground granulated blast furnace slag and waste clay brick, Cement and Concrete Composites 118 (2021) 103982, https://doi.org/10.1016/j.cemconcomp.2021.103982.
[37] D.Y. Lei, L.P. Guo, W. Sun, et al., A new dispersing method on silica fume and its influence on the performance of cement-based materials, Construction and Building Materials 115 (2016) 716–726.
[38] X. Chen, M. Zhou, W. Shen, G. Zhu, X. Ge, Mechanical properties and microstructure of metakaolin–based geopolymer compound–modified by polyacrylic emulsion and polypropylene fibers, Construction and Building Materials 190 (2018) 680–690.
[39] A. Hidalgo, S. Petit, C. Domingo, at al., Microstructural characterization of leaching effects in cement pastes due to neutralisation of their alkaline natüre Part I: Portland cement pastes, Cement and Concrete Research 37 (2007) 63–70.
[40] X. Huang, M. Jiang, X. Zhao, C. Tang, Mechanical properties and hydration mechanisms of high-strength fluorogypsum-blast furnace slag-based hydraulic cementitious binder, Construction and Building Materials 127 (2016) 137–143.
[41] S.M. Monteagudo, A. Moragues, J.C. Gálvez, et al., The degree of hydration assessment of blended cement pastes by differential thermal and thermogravimetric analysis, Morphological evolution of the solid phases, Thermochimica Acta 592 (2014) 37–51.
[42] B. Zhang, H. Tan, W. Shen, et al., Nano-silica and silica fume modified cement mortar used as Surface Protection Material to enhance the impermeability, Cement and Concrete Composites 92 (2018) 7–17.
[43] M. Bhattacharya, K.V. Harish, An integrated approach for studying the hydration of portland cement systems containing silica füme, Construction and Building Materials 188 (2018) 1179–1192.
[44] P. Türker, A. Yeğinobalı, Comparison of hydration products of different pozzolanic systems, Cement and Concrete, World 46 (2003) 52–66.
[45] J. Liu, Q.Q. Yu, Qingbo, The effect of size distribution of slag particles obtained in dry granulation on blast furnace slag cement strength, Powder Technology 362 (2020) 32–36.